Thermal convection in a cylinder and the problem of planform selection in an internally heated fluid layer

V. V. Kolmychkov, O. V. Shcheritsa, and O. S. Mazhorova[*]

Keldysh Institute of Applied Mathematics RAS, Miusskaya sq.4, Moscow, 125047, Russian Federation

(Received 31 March 2016; revised manuscript received 25 July 2016; published 29 December 2016)

The paper deals with the hexagonal convective flow near the stability threshold in an internally heated fluid layer. In our previous numerical study of convection near the stability threshold in a square box with internal heat generation [Phys. Lett. A **377**, 2111 (2013)] for a region of large horizontal extent, it has been shown that at small values of Prandtl number (Pr), convection sets in as a pattern of hexagonal cells with upward motion in the center (up-hexagons), whereas at large Pr, a stable flow pattern is formed by hexagonal cells with a downward motion in the center (down-hexagons). Here, we study axisymmetric convection in a cylinder as a model of motion in a single hexagonal cell. The radius of the cylinder matches the size of hexagons observed in our three-dimensional simulation. The lateral boundary of the cylinder is free and heat insulated. Horizontal bounding surfaces are rigid. The upper boundary is maintained at a constant temperature; the lower one is insulated. Two stable, steady-state motions with the upward and downward flow at the cylinder axis have been attained in calculations, irrespective of Pr. Cylindrical motion with the same direction of circulation as in the stable hexagons has a maximum temperature drop measured along the radius at the bottom of the cell. We suggest maximization of the temperature drop as a selection criterion, which determines the preferred state of motion in an internally heated fluid layer. This new selection principle is validated by the comparative analysis of the dominant nonlinear effects in low- and high-Prandtl number convection.

DOI: 10.1103/PhysRevE.94.063118

I. INTRODUCTION

Natural convection induced by internal heat generation plays an important role in many geophysical, astrophysical, industrial, and technological processes, such as mantle motion in the Earth [1], convection in atmosphere [2], fluid motion in crystal growth systems [3], and in nuclear reactor core [4]. Also, convection retained by internal heat sources is one of the most attractive pattern-forming systems with broken inversion symmetry where, in a scope of a sufficiently simple problem statement, a variety of steady flow patterns is physically realizable. Near the onset of motion, one can observe stable rolls, hexagonal cells with ascending (up-hexagons) and descending (down-hexagons) flow at the center, finite amplitude motion at Rayleigh number Ra below the threshold prescribed by linear stability theory. Prediction and elucidation of flow pattern formation induced by uniform internal heating contribute to the study of nonlinear processes in hydrodynamic stability. Usually, fluid arrangements with isothermal top boundary and adiabatic bottom are used for this purpose.

Such systems are controlled by two dimensionless parameters: standard Prandtl number $\mathrm{Pr} = \frac{\nu}{\varkappa}$, and the Rayleigh number proportional to the volume strength of heat source $\overline{q}$, $\mathrm{Ra} = \frac{g\beta\overline{q}d^5}{2\nu\varkappa^2}$, where d is the height of the fluid, g is the absolute value of the gravitational acceleration, $\beta = -\frac{1}{\rho}\frac{\partial\rho}{\partial T}$ is the thermal expansion coefficient, ρ is the fluid density, ν is the kinematic viscosity, and $\varkappa$ is the thermal diffusivity [5].

A number of theoretical, experimental, and numerical studies have addressed the stability of the convective structures in a layer with internal heat generation. (See, for example, Refs. [6–15]). Most of them are focused on convection at moderate and large Prandtl number and show the stability of finite amplitude down-hexagons in the subcritical domain and under slightly supercritical conditions.

A theoretical investigation performed by M. Tveitereid and E. Palm [16] deserves particular attention. For weakly nonlinear convection in an internally heated fluid layer, the authors predicted an effect of Prandtl number Pr on the process of planform selection. They found a critical value of Prandtl number $\mathrm{Pr}_{\mathrm{cr}} \approx 0.25$, such that at $\mathrm{Pr} > \mathrm{Pr}_{\mathrm{cr}}$ down-hexagons is the only stable planform. At $\mathrm{Pr} < \mathrm{Pr}_{\mathrm{cr}}$, the stable planform is up-hexagons. In the subcritical domain, at a fixed Rayleigh number $\mathrm{Ra} < \mathrm{Ra}_{\mathrm{cr}}$, the up- and down-hexagons exchange stability with the conductive state instead of rolls.

Our numerical study [17] is closely related to the investigation of Ref. [16]. We performed a full-scale computer simulation of convection in an internally heated fluid box, square in horizontal direction, with the aspect ratio 15. The calculations revealed stable flow patterns of up-hexagons at $\mathrm{Pr} < \mathrm{Pr}_{\mathrm{cr}}$, with down-hexagons being stable at $\mathrm{Pr} > \mathrm{Pr}_{\mathrm{cr}}$, and rolls near $\mathrm{Pr}_{\mathrm{cr}} \approx 0.25$. Transitions between the conductive state, rolls, up and down hexagonal flows were investigated for the Prandtl number in the range [0.1,100] and the Rayleigh number from subcritical values up to $1.5\mathrm{Ra}_{\mathrm{cr}}$. We predicted regions in the (Pr, Ra) plane, where different flow patterns are stable. The numerical results are consistent with theoretical deductions [16]. Nevertheless, the mechanics of planform selection is still unclear.

The purpose of this study is to gain a better understanding of the physical grounds for the preference of one or another flow pattern at different values of Prandtl number. We investigate the axisymmetric convection in a cylinder of appropriate size as a model of fluid motion in the regular hexagonal cell. The motion is induced by internal heat generation. The lateral boundary of the cylinder is free and heat insulated. Horizontal bounding surfaces are rigid. The upper one is maintained at a constant temperature, while the lower one is insulated. The approach is approved by the geometrical similarity between

[*]olgamazhor@mail.ru

the flow structure in a hexagonal cell and in a cylinder, the size of which allows us to inscribe the cylinder into a hexagonal cell. Such similarity has been noted by Rayleigh [18] and other investigators subsequently. Under weakly overcritical conditions, we achieved in calculation stable axisymmetric motions with the upward and downward flow at the axis, regardless of Prandtl number. The stability of the two motions subjected to the same Prandtl and Rayleigh numbers permits us to compare their temperature and velocity fields. From the comparison, we deduce a new criterion that determines the preferred direction of circulation in a hexagonal cell: the physically realizable motion has a maximum difference between the temperature at the axis and the outer boundary of the cell, measured at the bottom. This new selection principle is nonintegral, and in this sense, it is strongly different from the well-known integral ones proposed by W. Malkus [19,20], F. Busse [21], and E. Palm [22]. A physical interpretation of the suggested selection principle is provided.

II. PROBLEM STATEMENT

A. Governing equations

Convective motion of internally heated Boussinesq fluid is studied within a cylindrical region with the height d and radius $r_0 d$. The fluid motion is governed by the Navier-Stokes equations and heat conduction equation with uniform heat source term. For nondimensional description, the length is scaled with the height of the cylinder d, $t_v = d^2/\nu$ is a unit of time. Nondimensional temperature is introduced as $T = \frac{2(T_d - T_{\rm top})\kappa}{\bar{q} d^2}$, T_d is the dimensional temperature, $T_{\rm top}$ is the temperature of the upper boundary. Below, all functions and variables are nondimensional.

The flow is axisymmetric. In cylindrical polar coordinates (r,φ,z), the motion is constrained to be purely meridional, thus velocity $V = (V_r,0,V_z)$. Equations of motion are written in stream function-vorticity form. Vorticity Ω is the curl of the velocity and for axisymmetric motion $\Omega = (0,\Omega_\varphi,0)$. Since velocity field is solenoidal, stream function ψ can be chosen such that

$$V_r = \frac{1}{r}\frac{\partial \psi}{\partial z}, \quad V_z = -\frac{1}{r}\frac{\partial \psi}{\partial r}. \tag{1}$$

It is convenient to use $\omega = -\Omega_\varphi/r$, instead of Ω_φ. Then dynamic equation for ω is

$$\begin{aligned} r\frac{\partial \omega}{\partial t} + \frac{\partial}{\partial r}\left(\frac{\partial \psi}{\partial z}\omega\right) - \frac{\partial}{\partial z}\left(\frac{\partial \psi}{\partial r}\omega\right) \\ = \frac{\partial}{\partial r}\left[\frac{1}{r}\frac{\partial}{\partial r}(r^2\omega)\right] + \frac{\partial}{\partial z}\left[\frac{1}{r}\frac{\partial}{\partial z}(r^2\omega)\right] - \frac{\mathrm{Ra}}{\mathrm{Pr}}\frac{\partial T}{\partial r}. \end{aligned} \tag{2}$$

Kinematic equation connecting ψ and ω has the form

$$-r\omega = \frac{\partial}{\partial r}\left(\frac{1}{r}\frac{\partial \psi}{\partial r}\right) + \frac{\partial}{\partial z}\left(\frac{1}{r}\frac{\partial \psi}{\partial z}\right). \tag{3}$$

Heat conduction equation is

$$\begin{aligned} \frac{\partial T}{\partial t} + \frac{1}{r}\left[\frac{\partial}{\partial r}(r V_r T) + \frac{\partial}{\partial z}(r V_z T)\right] \\ = \frac{1}{\mathrm{Pr}}\frac{1}{r}\left[\frac{\partial}{\partial r}\left(r\frac{\partial T}{\partial r}\right) + \frac{\partial}{\partial z}\left(r\frac{\partial T}{\partial z}\right)\right] + \frac{2}{\mathrm{Pr}}. \end{aligned} \tag{4}$$

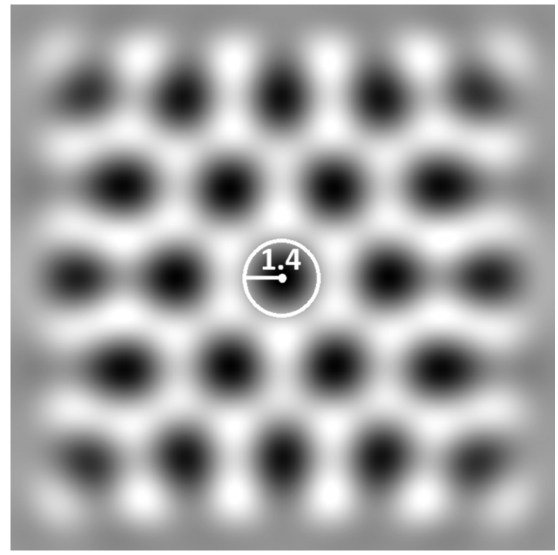

FIG. 1. The temperature field in the square box $15 \times 15 \times 1$ in the section $z = 0.5$. Results of our 3D calculations for Ra = 1420, Pr = 1 [17]. The temperature field displays a hexagonal cellular flow pattern. The size of the hexagon is approximately $2r_0$. Dark regions correspond to cold sinking fluid; in light regions, hot fluid is rising (down-hexagons).

Equations (2)–(4) are solved in the cylindrical region $0 \leqslant r \leqslant r_0, 0 \leqslant z \leqslant 1$.

The boundary conditions for the velocity field are no-slip on the rigid surfaces and tangential slip without any tangential stress on the cylindrical boundary, so that

$$\psi|_{z=0,1} = \left.\frac{\partial \psi}{\partial n}\right|_{z=0,1} = 0, \tag{5}$$

$$\psi|_{r=r_0} = \omega|_{r=r_0} = 0. \tag{6}$$

The temperature is fixed at $z = 1$, elsewhere on the boundary, heat flux vanishes:

$$T|_{z=1} = 0; \left.\frac{\partial T}{\partial z}\right|_{z=0} = \left.\frac{\partial T}{\partial r}\right|_{r=r_0} = 0. \tag{7}$$

At the axis, symmetry requires that

$$\psi|_{r=0} = \Omega_\varphi\Big|_{r=0} = 0; \left.\frac{\partial T}{\partial r}\right|_{r=0} = 0. \tag{8}$$

The radius of the cylinder r_0 is prescribed by the size of hexagonal cells observed in our three-dimensional (3D) simulation of a fluid flow induced by uniform heating in a rectangular box of height $h = 1$ and square in the horizontal direction. The aspect ratio of the box is 15. All boundaries are rigid; the vertical walls are perfectly insulated; as in the case with the cylinder, the upper boundary is maintained at constant temperature $T_{\rm top} = 0$, the lower boundary is adiabatic. At Rayleigh number near the stability threshold, we numerically obtained a steady flow pattern of regular hexagons (Fig. 1). Their size $r_0 = 1.4$ determines the radius of the cylinder.

The basic state of pure conduction is described by the stream function $\psi = 0$ and the reference temperature profile $T_0(z) = 1 - z^2$.

The initial conditions are determined by the basic state, with a perturbation of conductive temperature at the level $z = 1/3$:

$$\psi(r,z,0) = \omega(r,z,0) = 0, \tag{9}$$

$$T(r,z,0) = T_0(z) + A\varepsilon(r)\delta(z - 1/3), \tag{10}$$

where A is constant amplitude of the perturbation, $A > 0$, $\varepsilon(r)$ is a monotone function, $0 < \varepsilon < 1$, $\delta(z-1/3) = 0$ for $z\neq 1/3$ and $\delta(z-1/3) = 1$ for $z = 1/3$.

To initiate up-flow at the axis of the cell, perturbation with $\partial\varepsilon/\partial r < 0$ is imposed. By analogy with hexagonal motion, we call such flow pattern up-cell. Perturbation with $\partial\varepsilon/\partial r > 0$ activates opposite direction of circulation inside the cylinder. We call this flow arrangement down-cell.

The problem Eqs. (2)–(8) is solved by two-level implicit finite difference procedure specially designed for the numerical study of long-term convective motion in incompressible fluid [23]. Space-differencing of the advection terms in Eqs. (2) and (4) is done following Ref. [24]. At each time level, the Navier-Stokes equations and equation of heat transfer are solved in turn. First, the velocity field is determined. Then, velocity is inserted into the discretized Eq. (4) and the temperature is calculated. The algorithm for the equation of motion is based on a scheme, which conserves the mean kinetic energy [24]. Finite-difference equations for vorticity and stream function are solved by coupled algorithm with respect to the vector $X = (\omega,\psi)$. Boundary condition on vorticity is specified in Tom's form [25] and incorporates vorticity and stream function at the implicit time level. Under this approach, integral restriction on the vorticity [26] (conservation of vorticity), which is essential for the physical problem statement, is valid in the discrete model. Finite difference approximation of heat conduction equation ensures conservation of mean-square temperature [24]. Conservation of the quadratic means (the mean kinetic energy and square temperature) together with the integral constraint on the vorticity, provided by the coupled solution of the motion equations, make the numerical procedure very reliable in long-term numerical integration. Most of the calculations have been done on a spatial grid of the size 128×128 with time step $0.1t_\nu$. The results are practically insensitive to grid refinement.

B. Integral quantities

Let us consider volume averaged kinetic energy, $E = \frac{1}{2}\int_0^1\int_0^{r_0}(V_r^2 + V_z^2)rdrdz$, and vertical convective heat flux, $\langle V_zT\rangle = \int_0^1\int_0^{r_0} V_zTrdrdz$, of the steady-state fluid motion described by Eqs. (2)–(4) and boundary condition Eqs. (5)–(8). As described in Ref. [27], we relate $\langle V_zT\rangle$ to the boundary temperature. Multiplying Eq. (4) by $(z - 1/2)$ and integrating the result over the volume, the following equation is obtained:

$$\int_0^1\int_0^{r_0} V_zTrdrdz + \frac{1}{\mathrm{Pr}}\int_0^{r_0}\left[\frac{1}{2}\frac{\partial T}{\partial z}\bigg|_{z=1} + T(r,0)\right]rdr = 0. \tag{11}$$

Since integration of Eq. (4) yields

$$-\frac{1}{\mathrm{Pr}}\int_0^{r_0}\frac{\partial T}{\partial z}\bigg|_{z=1} rdr = \frac{r_0^2}{\mathrm{Pr}},$$

Eq. (11) can be rewritten in the form

$$\langle V_zT\rangle = \frac{1}{\mathrm{Pr}}\int_0^{r_0}[T_0(0) - T(r,0)]rdr; \tag{12}$$

i.e., volume-averaged vertical convective heat flux is completely defined by a deviation of the temperature from the reference value at the cylinder bottom.

Averaged heat flux as a selective factor for a realizable steady-state solution of the equations of motion was first conjectured by W. Malkus [19] and discussed thereafter in Ref. [20]. The author anticipated that the preferable convective flow pattern maximizes the heat transport. F. Busse displayed the equivalence between Malkus's selection principle and maximization of the kinetic energy in a stable solution [21]. It will be shown how these selection criteria work for the problem in hand.

III. NUMERICAL RESULTS

A. Stability map

Our numerical experiments estimate that the critical Rayleigh number, $\mathrm{Ra}^*_{\mathrm{cr}}$, for the considered axisymmetric problem is close enough to $\mathrm{Ra}^\infty_{\mathrm{cr}} = 1386$, suggested previously for an infinite horizontal layer [8], $\mathrm{Ra}^*_{\mathrm{cr}} \approx \mathrm{Ra}^\infty_{\mathrm{cr}} + 20$.

Under weakly overcritical conditions, namely, $\mathrm{Ra} = 1420, 1440$, and Prandtl number in the range $\mathrm{Pr}\in[0.01, 100]$, two steady-state solutions, one with up-flow and the other with down-flow at the center of the cell, were observed in the calculations. The direction of the circulation was determined by the initial temperature distribution. Thus, if the deterministic disturbance enhances the temperature toward the axis, $\partial\varepsilon/\partial r < 0$, steady-state motion has positive vertical velocity near the center ($r = 0$) and negative velocity near the lateral boundary ($r = r_0$). Conversely, if $\partial\varepsilon/\partial r > 0$, the steady flow is downward near the center and upward near the outer boundary.

In the subcritical domain $\mathrm{Ra}\in[\mathrm{Ra}_{\min}, \mathrm{Ra}^*]$, only one of these flows saves its stability. $\mathrm{Ra}_{\min}$ and direction of circulation in the unique stable motion depend on Pr. There is a critical Prandtl number $\mathrm{Pr}_{\mathrm{cr}}$, such that at $\mathrm{Pr} > \mathrm{Pr}_{\mathrm{cr}}$ down-cell is stable; up-cell is stable at $\mathrm{Pr} < \mathrm{Pr}_{\mathrm{cr}}$, $\mathrm{Pr}_{\mathrm{cr}} \approx 0.225$.

Regions in the (Pr, Ra) plane, where up- and down-cells are stable, resemble the stability map for hexagonal convection in a square box with internal heat generation [17]. At $\mathrm{Pr} > \mathrm{Pr}_{\mathrm{cr}}$ near the stability threshold, cylindrical and hexagonal motions with down flow in the center are, in a certain sense, preferable flow patterns: in a rectangular box, down-hexagon is the only stable planform both in subcritical and overcritical domains. In axisymmetric convection, the preference of down cells shows itself in the stability under subcritical conditions. In the same sense, cylindrical cells with upward flow in the center are preferred at $\mathrm{Pr} < \mathrm{Pr}_{\mathrm{cr}}$.

With regard to convection in a fluid with temperature-depended viscosity, Liang, Vidal, and Acrivos in Ref. [28] have shown that both "up" and "down" solutions are stable in a cylinder when $\mathrm{Ra} > \mathrm{Ra}_{\mathrm{cr}}$. Moreover, they predicted that only one of these solutions remains stable in the subcritical regime. Joseph [29] confirmed the result of Liang *et al.* in a more general statement of the problem. The remaining two

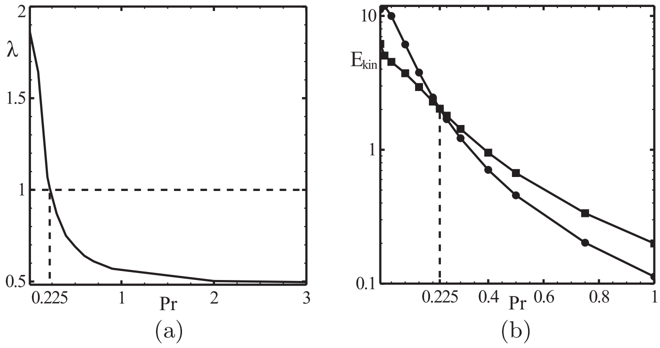

FIG. 2. Comparison of integral quantities in up and down cells. $Ra = 1420$. (a) The ratio between averaged convective heat fluxes in up-cell and down-cell (λ) as a function of Pr; (b) Kinetic energy versus Prandtl number. ●, E_{up}; ■, E_{dn}. Near $Pr = 0.225$ $\langle V_z T\rangle_{up} = \langle V_z T\rangle_{dn}$ and $E_{up} = E_{dn}$.

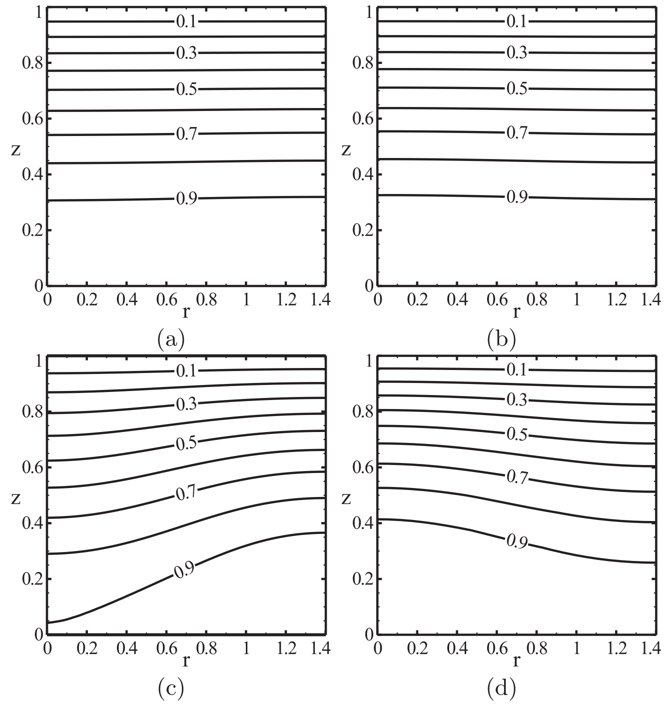

FIG. 3. Temperature field. Up-row: $Pr = 0.01$, (a) down-cell, (b) up-cell. Down-row: $Pr = 100$, (c) down-cell, (d) up-cell. At small Prandtl number, fluid motion produces small deviation of strait contour lines from horizontal. At large Prandtl number, curved isotherms display advection of temperature.

investigations [28,29] were restricted to the case of large Prandtl number.

B. Kinetic energy and convective heat flux

Mean convective heat flux $\langle V_z T\rangle$ has been calculated for steady motion in up- and down-cells under weakly overcritical conditions. To compare the effectiveness of convective heat transport in the flows with different directions of circulation, the ratio $\lambda = \langle V_z T\rangle_{up}/\langle V_z T\rangle_{dn}$ as a function of Prandtl number is plotted in Fig. 2(a). Here and below, subscripts "up" and "dn" denote quantities related to up- and down-cells, respectively. At small Prandtl number, motion with up-flow in the center maximizes averaged vertical convective heat flux, $\lambda > 1$. Near the critical Prandtl number, effectiveness of both flow patterns equalizes, $\lambda = 1$. For $Pr > Pr_{cr}$, motion with down flow along the cylinder axis produces maximum heat flux, $\lambda < 1$. According to Eq. (12), maximum vertical heat transport is associated with minimum averaged over the cylinder bottom temperature.

The kinetic energy displays similar behavior as vertical heat flux. Numerical data show that $E_{up} > E_{dn}$ for $Pr < Pr_{cr}$ and $E_{up} < E_{dn}$ for $Pr > Pr_{cr}$ [Fig. 2(b)].

The calculations reveal a significant extremum property of steady motions in the cylindrical cell. Flow, which rotates in the same direction as in the stable 3D hexagon, has maximum kinetic energy, and maximum averaged over the volume vertical convective heat flux.

Strictly speaking, Malkus's selection principle [19,20] and Busse's criterion [21] are not applicable to convection in a finite circular cylinder, where the two stable solutions with different transport capacities exist at $Ra > Ra_{cr}$. On the other hand, the maximum of the kinetic energy and averaged vertical heat transport indicates the unique solution, which is stable under subcritical conditions.

C. Temperature and velocity fields

Specific features of convective motion at small and large Prandtl number are determined by different dominant nonlinearities. For $Pr \gg 1$, the dominant nonlinear effect lies in advection of temperature isolines, while nonlinearity in hydrodynamic part is less important. In the case of $Pr \ll 1$, advection of velocity prevails since the main nonlinear terms come from Navier-Stokes equations.

Figure 3 shows the effect of Prandtl number on the temperature distribution. At $Pr = 0.01$, the temperature field is scarcely affected by convection. Isotherms are practically straight lines, and the temperature is very close to the pure conductive case. At $Pr = 100$, temperature is the quantity that is advected by the dominant nonlinear effects and isotherms are curved under the action of fluid motion.

The vertical component of the velocity field is plotted in Fig. 4. There are two bending points in the velocity field. The absolute value of V_z always has its maximum at the axis and minimum at the outer boundary. At low Prandtl number, nonlinear effects lead to a compression of vertical flux in the direction of motion: down flux becomes narrower approaching the cell bottom, while up-flux expands. The demarcation line between upward and downward motion, contour line $V_z(r,z) = 0$, is inclined toward the axis in up-cell and outward in down-cell. At large Prandtl number, the demarcation line is parallel to the cylinder axis.

Global properties of the motion manifest themselves in the velocity profiles near the cell bottom (Fig. 5). At $Pr = 0.01$, rising column of fluid in up-cell has a larger diameter than descending flux in down-cell, while at $Pr = 100$ vertical velocity in up- and down-cells changes its sign at the same point. At low Prandtl number, motion in up-cell is more intensive than in down cell and advection flattens velocity profile near the axis [Fig. 5(a)]. At high Prandtl number, nonlinear deformation of the velocity field is weak, profiles

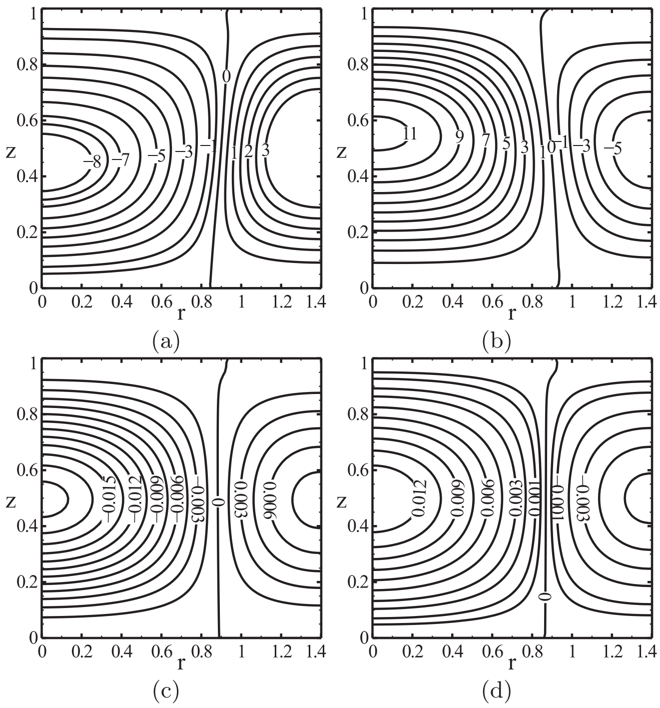

FIG. 4. Vertical component of the velocity. Up-row: $\mathrm{Pr} = 0.01$, (a) down-cell, (b) up-cell. Down-row: $\mathrm{Pr} = 100$, (c) down-cell, (d) up-cell. At $\mathrm{Pr} = 0.01$, z coordinates of velocity bending points are shifted. In the down-cell, minimum of V_z at the axis is located lower than the maximum on the outer boundary, and vice versa, maximum at the axis in up-cell is higher than the minimum at $r = r_0$. At $\mathrm{Pr} = 100$, bending points have the same vertical coordinate $z = 0.5$ both in up- and down-cells.

of vertical velocity near the bottom of up and down cells are similar and meet the level $V_z = 0$ at the same point [Fig. 5(b)].

Magnitudes of the velocity averaged over the axis and outer boundary is

$$V_z^{\varkappa}(r) = \mathrm{Pr}\int_0^1 V_z(r,z)dz,\ r = 0,\ r_0, \tag{13}$$

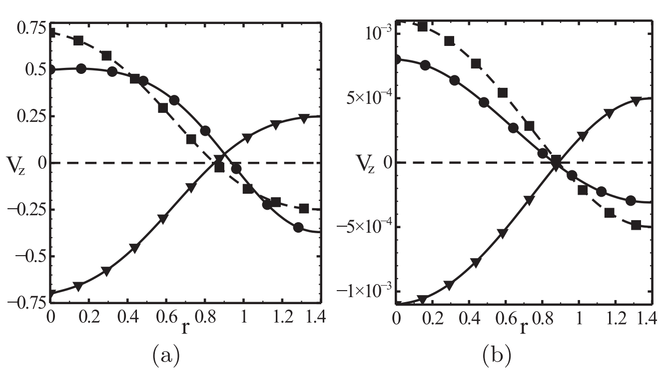

FIG. 5. Vertical velocity near the bottom (at $z = 0.06$) in up- and down-cells. (a) $\mathrm{Pr} = 0.01$; (b) $\mathrm{Pr} = 100$. Notice that near the axis absolute value of vertical velocity in down-cell is larger than velocity in up-cell both at $\mathrm{Pr} = 0.01$ and $\mathrm{Pr} = 100$. Profiles of V_z^{dn} and V_z^{up}, plotted against $-V_z^{\mathrm{dn}}$. ▼, V_z^{dn}; ●, V_z^{up}; ■, $-V_z^{\mathrm{dn}}$. Velocity is scaled with ν/d.

TABLE I. Averaged velocity $V_z^{\varkappa}$ and corresponding time interval $\Delta t_{\varkappa} = 1/V_z^{\varkappa}$.

Pr	0.01			
Cell	Up		Down	
r	0	r_0	0	r_0
$V_z^{\varkappa}$	6.1×10^{-2}	-3.1×10^{-2}	-4.6×10^{-2}	2.3×10^{-2}
$\Delta t_{\varkappa}$	16.4	31.12	21.45	42.33
Pr	100			
Cell	Up		Down	
r	0	r_0	0	r_0
$V_z^{\varkappa}$	7.2×10^{-1}	-2.8×10^{-1}	-9.9×10^{-1}	4.3×10^{-1}
$\Delta t_{\varkappa}$	1.39	3.51	1.006	2.3

and corresponding time intervals for a fluid particle to travel along the vertical boundaries, $\Delta t_{\varkappa} = 1/V_z^{\varkappa}, r = 0, r_0$ are given in Table I. (Here velocity is scaled with $\varkappa/d$.)

The data show that at $\mathrm{Pr} = 0.01$, fluid moves along the vertical boundaries very slowly on the thermal time scale. Under such conditions, the heat conduction has enough time to balance out the temperature and prevents the motion from distorting the parabolic temperature profile substantially [Fig. 6(a)].

At $\mathrm{Pr} = 100$, time interval for a particle to travel a distance of the cylinder height is near order of magnitude less than at $\mathrm{Pr} = 0.01$. Heat transport is dominated by fluid motion in this case. As a result, at the boundaries, we observe considerable departure of the temperature from the conductive profile [Fig. 6(b)].

D. Temperature distribution along the bottom of the cylindrical cell

Volume-averaged heat flux, which reaches its maximum in up-cell at $\mathrm{Pr} < \mathrm{Pr}_{\mathrm{cr}}$ and in down-cell at $\mathrm{Pr} > \mathrm{Pr}_{\mathrm{cr}}$, is strongly coupled with temperature distribution at the bottom of the cylinder [see Eq. (12)]. In this section, the effect of Prandtl

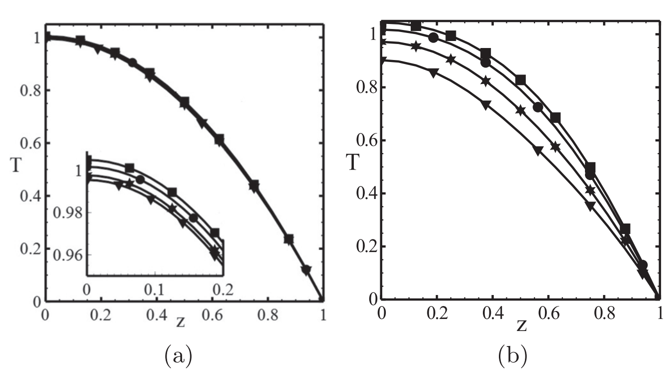

FIG. 6. Temperature profiles on the axis and outer boundary in up- and down-cells: (a) $\mathrm{Pr} = 0.01$, (b) $\mathrm{Pr} = 100$; ▼, down-cell, axis; ●, down-cell, boundary; ■, up-cell, axis; ✶, up-cell, boundary. The inset shows a noticeable deviation of the temperature profile from the reference one near the cylinder bottom at $\mathrm{Pr} = 0.01$.

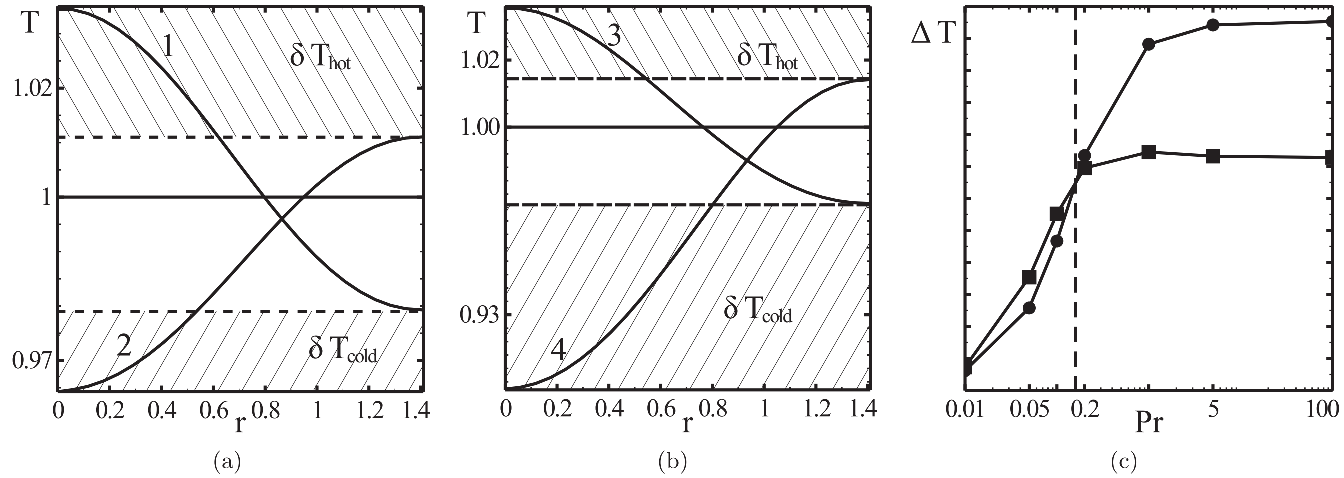

FIG. 7. Temperature distribution at the bottom. Ra = 1420. (a) Pr = 0.1; (1) $T^{\mathrm{up}}(r,0)$; (2) $T^{\mathrm{dn}}(r,0)$; (b) Pr = 100; (3) $T^{\mathrm{up}}(r,0)$; (4) $T^{\mathrm{dn}}(r,0)$; (c) The temperature drop between the axis and outer boundary; ●, down-cell; ■, up-cell. The magnitude of temperature drop in up- and down-cells increases with Pr number while Pr $\lesssim 2$, then settles approximately on constant.

number on the temperature field at the bottom of the cell is considered in detail.

Figure 7, where $T^{\mathrm{up}}(r,0)$ and $T^{\mathrm{dn}}(r,0)$ are plotted for Pr = 0.1 and Pr = 100, illustrates typical temperature distribution at small and large values of Prandtl number at the cylinder bottom. It is clearly seen that at small Prandtl number "cold" ends of the temperature profiles are closer than "hot" ones, i.e.:

$$\delta T_{\mathrm{cold}} < \delta T_{\mathrm{hot}}, \tag{14}$$

$$\delta T_{\mathrm{cold}} = T^{\mathrm{up}}(r_0,0) - T^{\mathrm{dn}}(0,0), \tag{15}$$

$$\delta T_{\mathrm{hot}} = T^{\mathrm{up}}(0,0) - T^{\mathrm{dn}}(r_0,0). \tag{16}$$

On the contrary, at large Prandtl number, temperature in the descending fluxes differs more than in uprising fluid:

$$\delta T_{\mathrm{cold}} > \delta T_{\mathrm{hot}}. \tag{17}$$

Inequalities Eqs. (14) and (17) can be rewritten in the form, which allows to compare the temperature drop between the axis and outer boundary at the bottom of the cylinder:

$$\Delta T^{\mathrm{up}} > \Delta T^{\mathrm{dn}} \quad \text{for small Pr}, \tag{18}$$

$$\Delta T^{\mathrm{dn}} > \Delta T^{\mathrm{up}} \quad \text{for large Pr}, \tag{19}$$

where

$$\Delta T^{\alpha} = |T^{\alpha}(0,0) - T^{\alpha}(r_0,0)|, \alpha = \mathrm{up}, \mathrm{dn}. \tag{20}$$

The dependence of the temperature drop on Prandtl number is presented in Fig. 7(c). Qualitative results Eqs. (18) and (19) are confirmed by corresponding numerical data given in Table II. At small Pr, calculations manifest maximization of the temperature drop in the up-cell, while at large Pr the maximum is registered in down-cell.

It is worth noticing that in our simulation kinetic energy and averaged heat flux in up- and down-cells are equal at Pr = 0.225 (Fig. 2); the temperature drop in both types of cells levels off at a little bit lower value. We do not know the exact reason for this discrepancy. Maybe there is an interval of Prandtl numbers where axisymmetric motions pertain to some specific properties and the situation resembles 3D cellular convection. In the 3D calculations [17], a band of Pr numbers near $\mathrm{Pr}_{\mathrm{cr}}$ where roll flow is preferred has been registered. Outside that band, the transition from rolls to down-hexagons occurs with increasing Pr. As the Prandtl number decreases, up-hexagons become predominant motion planform. We can't observe 2D rolls in our cylindrical domain, but an interval of Pr numbers where cells with both types of circulation are on equal terms can exist. Axisymmetric convection with Rayleigh and Prandtl numbers near critical values requires a special investigation. However, such an investigation is not essential for the purpose of this study.

To sum up, outside an immediate vicinity of critical Pr number, the maximum temperature drop, maximum kinetic energy, and averaged heat flux are observed in the cylindrical motion, which rotates in the same direction as in the stable hexagonal cell. Maximization of the temperature drop provides a nonintegral selective factor, which can't be formally obtained from integral extremum properties (see Sec. III B) under apparent and reasonable restrictions on temperature distribution.

IV. PHYSICAL INTERPRETATION

A. Cylindrical motion

The full-scale numerical simulation displays maximization of the temperature drop in the preferred flow motion. It would be interesting to predict this result on the grounds of qualitative physical considerations and simplified mathematical models. Such physical understanding, rather than pure calculations, can

TABLE II. Temperature drop at the bottom of cylindrical cell.

Pr	0.01	0.05	0.1	0.2	1	5	100
$10^2 \times \Delta T^{\mathrm{up}}$	0.73	3.54	5.52	6.95	7.45	7.32	7.28
$10^2 \times \Delta T^{\mathrm{dn}}$	0.62	2.58	4.67	7.04	10.82	11.42	11.53

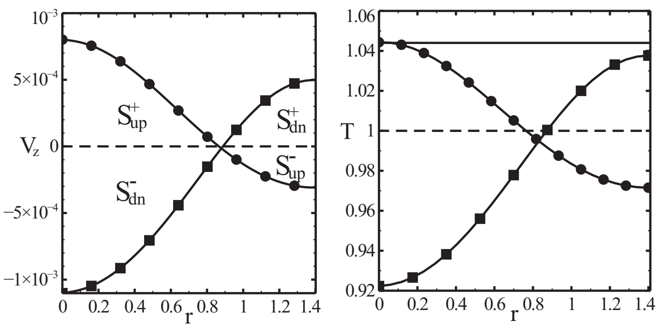

FIG. 8. Pr = 100. (a) Velocity distribution close to the bottom of the cylinder; (b) temperature distribution at the bottom of the cylinder; ■, down-cell; ●, up-cell

shed light on the problem of planform selection in Rayleigh-Benard convection.

At low Prandtl number and Rayleigh number close to $\mathrm{Ra}_{\mathrm{cr}}$, temperature field is controlled mainly by heat diffusion. Heat conduction has enough time to balance out temperature difference between the fluid element and its new surroundings. The temperature field is close to pure heat conduction profile. The velocity is small; its action on the temperature field is weak but still noticeable.

Under such conditions, 1D diffusion-dominated convection-diffusion problem Eqs. (A1) and (A2) provide simplified mathematical descriptions of the temperature distribution.

Now suppose both types of circulation in the cylinder are on equal terms. It means in particular that at the axis, absolute values of the averaged over z vertical velocity $|u_a|$ in up- and down-cells are equal, the same is true for the velocity at the outer boundary $|u_b|$, $|u_a| \ll 1$, $|u_b| \ll 1$, $u_a u_b < 0$. From geometrical consideration, it is obvious that velocity at the cell axis is higher than that at the lateral boundary: $|u_a| > |u_b|$. A reasonable estimate for the temperature drop ΔT^{α} Eq. (20) is given by the value of the temperature difference $\Delta Q(u_a,u_b)$, which is calculated in the Appendix. Equations (A5) and (A6) show that ΔQ at $u_a > 0$ is greater than ΔQ at $u_a < 0$. Therefore, at small Prandtl number, up-flow at the axis favors maximization of the temperature drop at the bottom of the cell.

Assessment of the temperature drop at high Prandtl number is based on the properties of the velocity field discussed in Sec. III C, namely, (P1) at the axis, near the bottom, absolute value of vertical velocity in down cell exceeds the velocity in up cell (Fig. 5), $|V_z^{\mathrm{dn}}(0,z)| > V_z^{\mathrm{up}}(0,z)$, $0 < z \leqslant \zeta < 0.4$; (P2) at a fixed z, vertical velocity in up and down cells as functions of r change their sign at the same point. Let it be that $r = \bar{r}$ and it is the only point, where $|V_z^{\mathrm{up}}(r,z)| = |V_z^{\mathrm{dn}}(r,z)|$, $z = \mathrm{const}$.

At high Prandtl number, velocity is comparatively large on the thermal time scale and advection has a substantial impact on the temperature field (Fig. 8). Quickly moving along the axis, cold flow in the down-cell does not have enough time for good heating. At the axis, near the bottom, the absolute value of vertical velocity in the down-cell exceeds the velocity in the up-cell (Fig. 5, 8(a); P1). Velocity directly affects the temperature, and at the axis near the bottom, temperature in the down-cell deviates from the reference profile more than that in the up-cell:

$$T_0(z) - T^{\mathrm{dn}}(0,z) > T^{\mathrm{up}}(0,z) - T_0(z), 0 \leqslant z \leqslant \zeta < 0.4. \tag{21}$$

Similar inequality is true at the outer boundary. Indeed, properties P1 and P2 ensure the following:

$$S_{\mathrm{dn}}^{-} > S_{\mathrm{up}}^{+}, \tag{22}$$

where (see Fig. 8)

$$S_{\mathrm{dn}}^{-} = \left|\int_0^{\bar{r}} r V_z^{\mathrm{dn}}(r,z)dr\right|;\ S_{\mathrm{up}}^{+} = \left|\int_0^{\bar{r}} r V_z^{\mathrm{up}}(r,z)dr\right|.$$

By virtue of the continuity equation,

$$S_{\mathrm{dn}}^{-} = S_{\mathrm{dn}}^{+};\ S_{\mathrm{up}}^{+} = S_{\mathrm{up}}^{-},$$

$$S_{\mathrm{dn}}^{+} = \left|\int_{\bar{r}}^{r_0} r V_z^{\mathrm{dn}}(r,z)dr\right|;\ S_{\mathrm{up}}^{-} = \left|\int_{\bar{r}}^{r_0} r V_z^{\mathrm{up}}(r,z)dr\right|.$$

Consequently,

$$S_{\mathrm{dn}}^{+} > S_{\mathrm{up}}^{-}. \tag{23}$$

Allowing for velocity property P2, integral inequality Eq. (23) means that $V_z^{\mathrm{dn}}(r_0,z) > |V_z^{up}(r_0,z)|$, and as well as near the axis, near the outer boundary temperature in down-cell deviates from the reference profile to a greater extent than that in the up-cell:

$$T^{\mathrm{dn}}(r_0,z) - T_0(z) > T_0(z) - T^{\mathrm{up}}(r_0,z), \quad 0 \leqslant z \leqslant \zeta. \tag{24}$$

Added together, Eqs. (21) and (24) give at $z = 0$

$$T^{\mathrm{dn}}(r_0,0) - T^{\mathrm{dn}}(0,0) > T^{\mathrm{up}}(r_0,0) - T^{\mathrm{up}}(r_0,0),$$

i.e., at high Prandtl number down flow at the axis is preferred for the maximization of the temperature drop at the cell bottom.

B. Hexagonal motion

Specific features of the motions essential to the physical interpretation of the selective factor are the same in cylindrical and hexagonal cells. Our 3D numerical simulation of hexagonal convection in a rectangular box of large horizontal extent (see Sec. II A) displays the likeness. For example, averaged time interval $\Delta t_{\varkappa}$ for a fluid element to move along the axis and outer boundary of the stable up-hexagon at $\mathrm{Pr} = 0.01$ is about $25t_{\varkappa}$ and $75t_{\varkappa}$, respectively. At these time scales, heat conduction flattens out the temperature in the horizontal direction. Nonlinear effects are mainly associated with the equations of motion. Consequently, at small Prandtl number, as in the axisymmetric case, 1D model Eqs. (A1) and (A2) are suitable for the qualitative analysis of the temperature field in hexagons. At $\mathrm{Pr} = 100$, on the axis of down-hexagon $\Delta t_{\varkappa} \approx t_{\varkappa}$, and on the lateral boundary, $\Delta t_{\varkappa} \approx 3t_{\varkappa}$. At large Prandtl number, dominant nonlinearity lies in advection of temperature isolines. Figure 9 shows that the departure of the temperature from the reference level $T_0(0) = 1$ at the bottom of down-hexagon ($\mathrm{Pr} = 100$) exceeds the appropriate value in up-hexagon ($\mathrm{Pr} = 0.01$) by more than an order of magnitude.

The similarity between the velocity fields in cylindrical and hexagonal cells is illustrated in Fig. 10, where contour lines of 3D vertical velocity are plotted in a plane passing through the axes of two adjacent hexagonal cells.

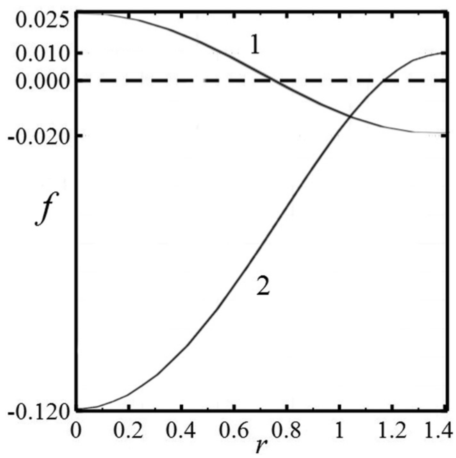

FIG. 9. Departure of the temperature from the reference point at the bottom of hexagonal cells, $f(r) = T(r,0) - T_0(0)$; based on the results of our 3D calculations. (1) up-hexagon, $\mathrm{Pr} = 0.01$, $f(r) \times 10$; (2) down-hexagon, $\mathrm{Pr} = 100$, $f(r)$.

At small Prandtl number, we notice in up-hexagon the compression of fluid flux in the direction of motion. As well as in the cylinder with ascending flow at the center, demarcation line $V_z = 0$ is inclined to the axis of up-hexagon [Fig. 10(a)]. At large Prandtl number, contour line $V_z = 0$ is parallel to the cell axis both in down-hexagon [Fig. 10(b)] and in the cylinder. The latter is the key point in using the mass conservation law for the estimation of the temperature drop at the bottom of the cell.

V. SELECTION CRITERIA

A close resemblance between fluid motion in the cylinder and hexagonal cell leads to the conclusion that a selective factor, which indicates the preferred (i.e., stable both in subcritical and overcritical domains) type of the motion in the cylinder equally pertains to hexagonal motions. Therefore, the selection criterion for physically realizable planform near the stability threshold in a fluid layer with internal heat generation, isothermal upper boundary, and adiabatic lower one reads as follows: subjected to the same Ra and Pr numbers, a stable flow pattern maximizes the absolute value of the difference between the temperature at the axis and the lateral boundary of a hexagonal cell. The temperature drop is measured at the bottom of the cell.

The proposed selection principle can be easily generalized to a fluid arrangement with another thermal boundary condition. As an example, we have investigated convection in a cylinder with rigid horizontal boundaries maintained at a constant temperature and correspondent 3D motion in a box. (Similar flow arrangement has been considered in Refs. [13,27].) Homogeneous heat generation produces conduction profile with an unstable temperature gradient in the upper part of the region and stable fluid stratification near the lower boundary. In this case, the effect of Prandtl number on the motion stability is the same. Stable up-hexagons have been observed at $\mathrm{Pr} < \mathrm{Pr}_{\mathrm{cr}}$, while down-hexagons are preferred at $\mathrm{Pr} > \mathrm{Pr}_{\mathrm{cr}}$, in the cylinder both directions of circulation are stable. The axisymmetric flow, which rotates in the same direction as in the stable hexagons, has maximum kinetic energy, averaged vertical heat flux, and the temperature drop. However, the temperature drop should be measured near the boundary between stably and unstably stratified fluid, at $z = 0.5$ or somewhere near this level.

In our calculations, we have found that temperature drop in the up and down cylindrical cells are equal at $\mathrm{Pr}_{\mathrm{cr}} \approx 0.225$ (Fig. 2). In 3D convection, both types of hexagons lose their stability in the vicinity of $\mathrm{Pr}_{\mathrm{cr}} \approx 0.25$ and rolls become the preferred state of motion [17]. Critical Prandtl number in the Benard-Marangoni convection is near the same [30]. We cannot suggest any physical reasons why the Prandtl number values around $\mathrm{Pr} = 0.25$ are crucial for the process of planform selection in different flow arrangement with broken inversion symmetry.

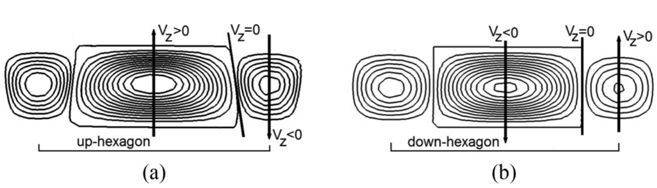

FIG. 10. Vertical velocity contour lines in a plane passing through the axis of two adjacent hexagons; (a) stable up-hexagon, $\mathrm{Pr} = 0.01$; (b) stable down-hexagon, $\mathrm{Pr} = 100$. Results of our 3D calculations.

VI. CONCLUSIONS

The paper contributes to the investigation of the problem of planform selection in the internally heated fluid. The study concerns the stability of up- and down-hexagons at large and small Prandtl numbers. We have considered axisymmetric motion in the cylinder of appropriate size as a model of a hexagonal cell. The cylindrical domain has stress-free and heat-insulated lateral boundaries. Direct numerical simulation of axisymmetric motion has been done near the stability threshold for Pr number in the range [0.01,100]. In the calculations, under slightly overcritical conditions, we obtained two stable solutions, one with up-flow and the other with down-flow at the cylinder axis, regardless of Pr number.

Flows, which rotate in the same direction as in the stable 3D hexagonal cell, have maximum kinetic energy, and maximum averaged convective heat flux. Up-cell possesses these extremum properties at $\mathrm{Pr} < \mathrm{Pr}_{\mathrm{cr}} \approx 0.25$, and down-cell exhibits the extremum properties at $\mathrm{Pr} > \mathrm{Pr}_{\mathrm{cr}}$. Under subcritical conditions, only motion with maximum kinetic energy and heat flux retains stability.

The comparative study of the flows with the different directions of circulation reveals one more extremum property of the preferred flow pattern: the maximum value of the temperature drop at the bottom of the cell. Maximization of the temperature drop does not stem directly from the averaged flow properties; nevertheless, it is approved by the distinct dominant nonlinear effects in small and large Prandtl number convection. Nonlinearities equally affect the flow, both in the cylindrical cells and in the 3D hexagons, and favor stability of up-hexagons at low Pr numbers and down-hexagons at high Pr numbers. Because of this similarity, we put forward maximization of the temperature drop as a new nonintegral selection principle for physically realizable convective motion in the internally heated fluid. The principle can be generalized to different boundary conditions.

ACKNOWLEDGMENTS

This work was supported by the Russian Foundation for Basic Research (Project No. 15-01-03741), by the Presidium of the Russian Academy of Sciences (basic research program no. 5).

APPENDIX

At small Prandtl number, temperature distribution along coordinate z can be qualitatively described by a solution of the following 1D convection-diffusion problem:

$$\frac{d^2Q}{dz^2} - u\frac{dQ}{dz} + 2 = 0, \quad z \in (0,1), \tag{A1}$$

$$\left.\frac{dQ}{\partial z}\right|_{z=0} = 0, \; Q|_{z=1} = 0, \tag{A2}$$

where u is constant. Its magnitude lies in the range, which is determined by the averaged vertical velocity Eq. (13) from Table I, $u \in [-0.5\times10^{-2}, 6.5\times10^{-2}]$, with $u < 0$ corresponding to down-flowing fluid in our 2D model and $u > 0$ representing the up-flowing flux.

The solution of Eqs. (A1) and (A2) is

$$Q(z,u) = \frac{2}{u}(z-1) - \frac{2}{u^2}(e^{uz} - e^{u}). \tag{A3}$$

Let us determine the deviation of $Q(z,u)$ from reference profile at $z = 0$:

$$\delta Q(u) = |T_0(0) - Q(0,u)| \approx \frac{1}{3}|u|\left(1 + \frac{u}{4}\right). \tag{A4}$$

Here, expansion of $Q(0,u)$ in powers of u has been used.

The following statements are easily derived from Eq. (A4):

(1) if two values of the velocity, u_a and u_b, have the same sign and $|u_a| > |u_b|$, then $\delta Q(u_a) > \delta Q(u_b)$;

(2) if $u_a > 0$, then $\delta Q(u_a) > \delta Q(-u_a)$;

Propositions (1) and (2) reveal that departure of $Q(u)$ from reference point $T_0(0)$ increases with $|u|$ and that the velocity of the same magnitude produces a greater departure from the reference value in the up-flowing fluid than in descending flux.

Further, from Eq. (A4) or directly from Eq. (A3), we can evaluate the temperature drop for given magnitudes u_a and u_b:

$$\Delta Q(u_a,u_b) = |Q(0,u_a) - Q(0,u_b)| \approx \frac{1}{3}|u_a - u_b|\left[1 + \frac{(u_a+u_b)}{4}\right], \tag{A5}$$

and notice that if $|u_a| > |u_b|$, then

$$\Delta Q(|u_a|, -|u_b|) > \Delta Q(-|u_a|, |u_b|). \tag{A6}$$

[1] D. L. Turcotte and G. Schubert, *Geodynamics* (Cambridge University Press, Cambridge, 2001), p. 848.

[2] K. A. Emanuel, *Atmospheric Convection* (Oxford University Press, Oxford, 1994), p. 592.

[3] S. Dost and B. Lent, *Single Crystal Growth of Semicomductors from Metallic Solutions* (Elsevier, New York, 2007), p. 493.

[4] D. L. Seung, K. L. Jong, and Y. S. Kune, Nucl. Eng. Des. **237**, 473 (2007).

[5] G. Z. Gershuni and E. M. Zhukhovitskii, *Convective Instability of Incompressinble Fluids* (Nauka, Moscow, 1972), p. 392.

[6] R. Krishnamurti, J. Fluid Mech. **33**, 445 (1968).

[7] R. Krishnamurti, J. Fluid Mech. **33**, 457 (1968).

[8] P. H. Roberts, J. Fluid Mech. **30**, 33 (1967).

[9] D. J. Tritton and M. N. Zarraga, J. Fluid Mech. **30**, 21 (1967).

[10] Y. Tasaka, Y. Kudo, Y. Takeda, and T. Yanagisawa, J. Phys.: Conf. Ser. **14**, 168 (2005).

[11] J. Takahashia, Y. Tasaka, Y. Muraia, Y. Takeda, and T. Yanagisawa, Int. J. Heat Mass Transf. **53**, 1483 (2010).

[12] G. C. Glover and S. C. Generalis, Eng. Appl. Comput. Fluid Mech. **3**, 164 (2009).

[13] S. C. Generalis and F. H. Busse, in *Proceedings Fifth European Thermal-Sciences Conference*, edited by G. G. M. Stoffels, T. H. van der Meer, and A. A. van Steenhoven (Eindhoven University of Technology, Eindhoven (NL), 2008), FCV 10.

[14] G. Cartland-Glover, K. Fujimura, and S. Generalis, Int. J. Nonlinear Sci. **2013**, 19 (2013).

[15] F. H. Busse, Eur. J. Mech. B Fluids **47**, 32 (2014).

[16] M. Tveitereid and E. Palm, J. Fluid Mech. **76**, 481 (1976).

[17] V. V. Kolmychkov, O. S. Mazhorova, and O. V. Shcheritsa, Phys. Lett. A **377**, 2111 (2013).

[18] Rayleigh, Phil. Maz. S.6 **32**, 529 (1916).

[19] W. Malkus, Proc. R. Soc. A, London **225**, 196 (1954).

[20] W. Malkus and G. Veronis, J. Fluid Mech. **4**, 225 (1958).

[21] F. H. Busse, J. Fluid Mech. **30**, 625 (1967).

[22] E. Palm, Int. J. Heat Mass Transf. **15**, 2409 (1972).

[23] O. S. Mazhorova and Y. P. Popov, Zh. Vychisl. Mat. Mat. Fiz. **20**, 1005 (1980).

[24] A. Arakawa, J. Comput. Phys. **1**, 119 (1966).

[25] A. Thom, Proc. R. Soc. A, London **141**, 651 (1933).

[26] C. Fletcher, *Computational Techniques for Fluid Dynamics*, Vol. 2, 2nd ed., Springer Series in Computational Physics (Springer-Verlag, Heidelberg, 1991), p. 515.

[27] D. Goluskin and E. A. Spiegel, Phys. Lett. A **377**, 83 (2012).

[28] S. F. Liang, A. Vidal, and A. Acrivos, J. Fluid Mech. **36**, 239 (1969).

[29] D. D. Joseph, J. Fluid Mech. **47**, 257 (1971).

[30] A. Thess and M. Bestehorn, Phys. Rev. E **52**, 6358 (1995).